Department of Chemistry
University of Eastern Finland

103/2010

Tiina Rasilainen

Controlling water on polypropylene surfaces with micro- and micro/nanostructures

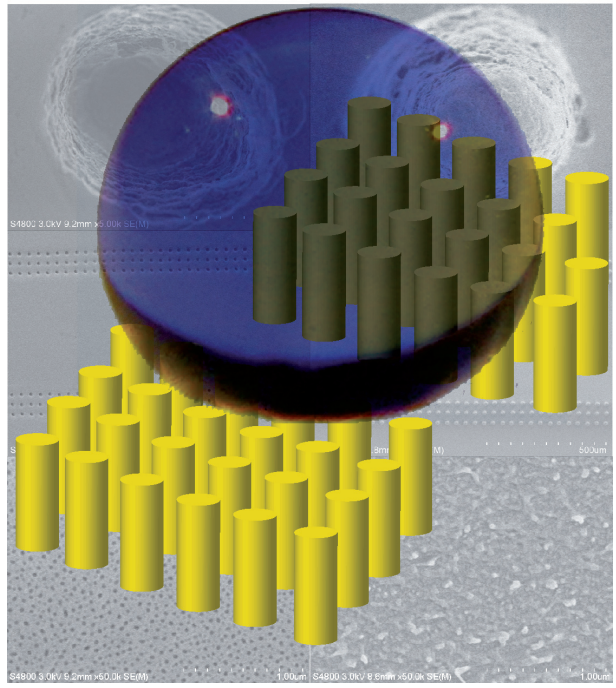

Controlling water on polypropylene surfaces with micro- and micro/nanostructures

Tiina Rasilainen

Department of Chemistry
University of Eastern Finland
Finland

Joensuu 2010

Tiina Rasilainen
Department of Chemistry, University of Eastern Finland
P.O. Box 111, 80101 Joensuu, Finland

Supervisor
Prof. Tapani Pakkanen, University of Eastern Finland

Referees
Prof. Jouni Pursiainen, University of Oulu
Prof. Raimo Alen, University of Jyväskylä

Opponent
Docent Leena Hupa, Åbo Akademi University

To be presented with the permission of the Faculty of Science and Forestry of the University of Eastern Finland for public criticism in Auditorium F100, Yliopistokatu 7, Joensuu, on December 17th, 2010 at 12 o'clock noon.

ISBN 978-952-61-0275-7
ISBN 978-952-61-0276-4 (PDF)

Kopijyvä Oy
Joensuu 2010

ABSTRACT

During recent years, surface structuring has become a common method to modify the surface properties of materials. Especially fabrication of biomimetic micro-, nano- and hierarchical structures in polymers has gained attention when aiming to create water-repellent and self-cleansing surfaces. In this work, polypropylene surfaces were furnished with several types of micro- and hierarchical micro/nanostructures, and contact and sliding angles of water were measured. Protrusive structures comprised micropillars or micropillars covered with nanobumps. On some surfaces, the pillars were arranged isotropically, on the rest the patterns were anisotropic, with parallel stripe- or zone-like structures. Hollow structures were isotropic and consisted of micropits or of micropits covered with nanodepressions.

Wetting properties of surfaces were investigated with contact and sliding angle measurements. Pillar structures on polypropylene increased the hydrophobicity of the material. With hierarchical isotropic structures, the superhydrophobic region was reached, and even with isotropic microstructures a clear increase was achieved in contact angles and decrease in sliding angles. On stripe- and zone-like surfaces, behaviour was anisotropic with direction-dependent contact and sliding angles. With proper parameters and hierarchical micro/nanostructures, stripe-like surfaces also showed superhydrophobicity. Pitted structures increased the contact angles, and with hierarchical micropits/nanodepressions, contact angle values were near the superhydrophobic limit.

All structures were fabricated by injection moulding. Aluminium foils were microstructured with a micro-working robot and further processed to obtain appropriate mould inserts for different structure types. For hierarchical structures, the aluminium foils were anodized to aluminium oxide patterned with microdepressions and nanopores. For pit structures, a novel fabrication method was developed where the pillar-structured mould inserts were fabricated by cold mounting of epoxy resin on structured aluminium or aluminium oxide foils. Dimensions and patterns of the polypropylene structures could be planned and controlled with the working parameters of the micro-working robot.

LIST OF ORIGINAL PUBLICATIONS

This dissertation is a summary of the following original publications I-IV.

I Puukilainen, E., Rasilainen, T., Suvanto, M., Pakkanen, T. A., Superhydrophobic Polyolefin Surfaces: Controlled Micro- and Nanostructures, *Langmuir* **23** (2007) 7263.

II Rasilainen, T., Suvanto, M., Pakkanen, T. A., Anisotropically microstructured and micro/nanostructured polypropylene surfaces, *Surface Science* **603** (2009) 2240.

III Rasilainen, T., Kirveslahti, A., Nevalainen, P., Suvanto, M., Pakkanen, T. A., Modification of polypropylene surfaces with micropits and hierarchical micropits/nanodepressions, *Surface Science* **604** (2010) 2036.

IV Rasilainen, T., Kirveslahti, A., Nevalainen, P., Suvanto, M., Pakkanen, T. A., Controlling the movement of water droplets with micro- and hierarchical micro/nanostructures, submitted for publication.

CONTENTS

SYMBOLS AND ABBREVIATIONS

AAO	Anodized aluminium oxide
bPE	Poly(ethylene-1-butene) copolymer
CA	Contact angle
para	Parallel
perp	Perpendicular
PFPE	Perfluoropolyether
PP	Polypropylene
r	Roughness factor
SA	Sliding angle
SEM	Scanning electron microscopy
γ	Interfacial free energy
θ	Contact angle of water
ϕ_s	Area fraction

1 INTRODUCTION

Water-repellent and self-cleansing properties of the plant world have attracted attention for hundreds or even thousands of years. The "sacred lotus" was mentioned in early Sanskrit writings[1] and many other plants possess similar features[1,2]. Rice leaves[3,4] can even control the movement of water, directing droplets to flow parallel to leaf edges. The animal world, too, has its share of these properties: Butterflies[5] direct water to flow away from their body, water striders[6] can skate on water and desert beetles[7] use structures on their shells to trap water droplets from fog.

As microscopy techniques have developed, the fascinating world of micro-, nano- and hierarchically scaled structures with their extraordinary wetting properties has been revealed[1]. An increasing number of researchers are now channelling their interest to the creation of artificial surfaces with biomimetic structures and hydrophobic properties. A diversity of materials and techniques have proven to be applicable for surface structuring[8-11]. Polymers have become popular because they tend to be cost-efficient, can be handled with several techniques, and are suitable for mass production[3,12-33]. Hydrophobic polymer surface that also allow control of the movement of water droplets would find use in many areas, from diagnostics and research to everyday household items.

1.1 HYDROPHOBICITY AND CONTACT ANGLES

The scientific principles behind hydrophobicity have been under investigation for at least two centuries, ever since Young presented his equation for the contact angle of a liquid drop on a smooth surface:[34]

$$\cos\theta = \frac{\gamma_{SV} - \gamma_{SL}}{\gamma_{LV}}, \qquad (1)$$

where γ_{SV}, γ_{SL} and γ_{LV} are the interfacial free energies per unit area of the solid–vapour, solid–liquid and liquid–vapour interfaces. Young's equation gives the contact angle of the drop when it is in equilibrium state with minimum energy[34,35] (see Figure 1).

If θ is < 90°, the surface is said to be hydrophilic. With values > 90°, surfaces are hydrophobic.[3,36] There are some studies that suggest the hydrophobic limit should be 65°, but prevailing opinion is in favour of the traditional 90° [37,38]. If the contact angles are >150° and the sliding angles (tilting angle of the surface at which drops begin to slide or roll) are < 10°, the surfaces are defined as superhydrophobic.[3,36] The lowest energy and highest θ reported for a smooth surface are for a hexagonally arranged CF_3 surface, where the contact angle is 119° [39]. For higher contact angles, the surfaces need to be roughened[34,40].

Wenzel modified Young's equation for contact angles on rough surfaces, when the drop has adopted the Wenzel state (Figure 1) and adapts to follow the shape of the surface structures[34,35,40,41]:

$$\cos\theta^* = r\cos\theta, \qquad (2)$$

where θ is Young's contact angle and r is the roughness factor, calculated as the ratio of the actual area to the geometric area of the surface on which the drop rests.[34,35,40,41]

Cassie and Baxter proposed a second possible state for the drop, in which it rests on top of the asperities of a rough surface. In Cassie-Baxter state, the contact angle is calculated with the Cassie-Baxter equation[34,35,41,42]

$$\cos\theta^* = -1 + \phi_s(\cos\theta + 1), \qquad (3)$$

where θ is Young's contact angle and ϕ_s refers to the area fraction, the ratio of the asperity tops to the geometric area of the surface.[34-35,41-42] States between Wenzel and Cassie-Baxter, where the drops partially wet the asperities, are also possible[13]**.** Figure 1 depicts Young's contact angle and the Wenzel and Cassie-Baxter states.

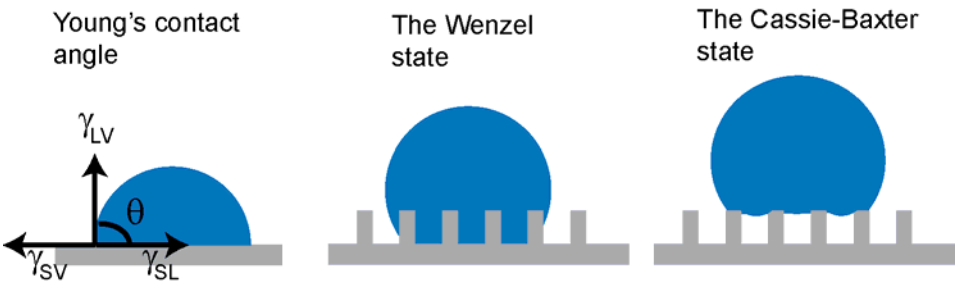

Figure 1. Young's contact angle and the Wenzel and Cassie-Baxter states.

Calculations have been made and experiments done to develop criteria for hydrophobic surface structures[17,20,34,43-50]. It has been shown that superhydrophobicity requires the Cassie-Baxter state, where the drop rests on the composite interface formed by the asperity tops and air between. A composite interface reduces the contact area between solid and liquid, leading to decreased adhesion, increased contact angles and easy sliding.[20,43-45,49,51-55] The Cassie-Baxter state tends to be metastabile and represent a local, not global, energy minimum[26,53-54,56,57]. It can be moderately robust, nevertheless, and

the properties of lotus leaves have been shown to stem from metastability[53]. Transitions from metastabile Cassie-Baxter to stable Wenzel state have also been observed[26,46,57,58].

Surfaces can be roughened with micro- or nanometer-sized structures, or by combining the different scales into one hierarchical structure. As several theoretical[19,43-45,51-53,55] and experimental[2,4,6,16,19,20,22,28,33,46,54,59-61] studies have confirmed, the hierarchical structure where droplets are in Cassie-Baxter state is essential for superhydrophobic surfaces. The composite interface that is formed in Cassie-Baxter state may be fragile and become destabilised by a number of factors, such as capillary waves, condensation of nanodroplets and surface inhomogeneities. The destabilising factors are scale-dependent, and multi-scale structures − hierarchically ordered micro- and nano-sized asperities − are needed to resist them effectively.[55]

Wenzel and Cassie-Baxter equations give just one contact angle, the static one, for the surface[41]. Experimentally, static angles are measured by carefully placing a drop on the surface. Although this is a widely used method, it may lead to overestimations of the hydrophobicity, since a gently placed drop easily adopts a metastabile state with high contact angle and energy[17,41,48,57,62,63]. The other way to measure contact angles is the dynamic angle method, where the volume of the drop on the surface is first increased and then decreased. The increasing step gives the advancing contact angle and the decreasing step the receding one. Advancing and receding values are said to represent the highest and lowest possible angles.[56] For superhydrophobic surfaces with low sliding angles,[16,34,35,48,56,58,62-65] both the advancing and receding angles should be high and their hysteresis (their difference) low. Again, hierarchical structure outperforms one-scaled asperities: for both high CA and low hysteresis, a composite interface is required and, for that, the stabile Cassie-Baxter state that only hierarchical structures can provide.[55]

Theoretical calculations have mostly been done for isotropic surfaces where the asperities are homogeneously arranged and the shape of drops on the surfaces is symmetrical. On anisotropic surfaces the situation is different. For example, if the surface structure is stripe-like, with parallel ridges and grooves, drops will tend to elongate parallel to the grooves and be squeezed perpendicular to them, with the result that contact angles vary with the viewing direction.[35,58,66-76] With hierarchical anisotropic surfaces, the superhydrophobic effect may override the anisotropic effect and the drops maintain their spherical shape[77].

Applying the Wenzel and Cassie-Baxter equations to anisotropic surfaces is complicated and there are different theories and methods for calculating the roughness factors and area fractions[16,43,50,78-82]. There has even been some discussion as to whether the Wenzel and Cassie-Baxter equations are applicable at all to anisotropic surfaces or dynamic contact angles[47]. Predictions of the anisotropic effect and dynamic contact angles based on these equations have nevertheless been made[55,83,84], and some of the predictions have been in line with experimental results[61,66,85-86].

1.2 STRUCTURED POLYMER SURFACES

In aiming to create artificial superhydrophobic polymer surfaces, a logical approach has been to copy natural structures. The replication accuracies of the copying methods have been good and contact angles on the replicated surfaces high. But the accuracy has also been a weakness: the methods have not allowed modification of the structures, nor variation in the dimensions to determine whether the contact angles could be further increased.[12-15]

Several studies have been made and methods developed to fabricate structures that are biomimetic but not straight copies from nature. One of the first attempts was a fractal-like surface[87]. Isotropic pillar-like micro- or submicrostructures on polymers[16-20] have been fabricated by litography[19,20], plasma polymerisation[16], etching[16] and hot embossing[18]. For nanostructured polymer surfaces, a template method with a foil of anodized aluminium oxide as mask has proven useful[3,21-25]. Interesting nanostructured surfaces of fluorinated polymer blends[26] have been fabricated.

To truly mimic natural surface structures and achieve the water-repellent properties of plants[1-2] and animals[5-7], it has been of interest to combine the micro- and nanoscales into a hierarchical structure. Nanostructures on polymer microstructures have been produced by plasma treatment[20] and with interference lithography[27]. A catalytic one-step method has been used for preparation of micro/nano-structured polyethylene film[28], and hierarchical polymer structures have been achieved by electrohydrodynamics[29], nanoimprint lithography combined with X-ray lithography[30], and micromoulding together with phase inversion[31]. Anodized aluminium oxide has proven useful for the creation of micro/nanostructures. AAO foils with microdepressions covered with nanopores have been obtained by anodizing aluminium foils structured by sandblasting[32], photolitography[33] and imprinting[22]. The AAO foils are then used to structure polymers by moulding techniques[22,32,33].

Besides the creation of surfaces with high contact angles, there has been a growing interest to combine anisotropy with superhydrophobicity. With anisotropic surfaces, i.e. surfaces where the structures and contact angles are direction-dependent, it would be possible to guide the sliding direction of water droplets and to make paths over surfaces, as on rice leaves.[3,4,35] Micro-sized[66,68,83,85] and nano-sized[67] parallel grooves and ridges and anisotropically arranged micro-sized pillar-like[83,88] structures, more complex patterns[88] and structures with winding grooves[89], have been prepared by several techniques, amongst which lithography-based techniques[67,83,88] have been particularly popular. Hierarchical anisotropic polymer structures[77,86] have been prepared, as well, but if the surfaces are very hydrophobic the anisotropic effect may be lost[77].

In contrast to the wide variety of pillar structures in nature, hollow pit- or hole-like structures are rare. Artificial hollow structures on polymers have nevertheless begun to draw attention because of their potential applications in microdiagnostic[90] and drug-delivery[91] systems, in microchips for the separation of biomolecules[92,93], in micro-sized

electrodes[94] and devices[95-97] and in arrays for studies of liquid−liquid interfaces[98-100]. Developments in optical recording techniques are also dependent on microgratings and micropits[101-103], and water and oil can be separated with micro-sized mesh[104]. A variety of fabrication methods for one-scale hollow structures have been developed, including electron beam writing for nanopits and nanochannels[102,103] and laser ablation for micropits[90,94,98-100,105-108]. No reports of hierarchical hollow structures or the wettability of pit-like surfaces had been published before this work.

Common to the fabrication methods for protrusion and hollow structures is that they typically require expensive equipment or time-consuming processing steps, or both. Moreover, methods that can be used to create structures for research purposes may be challenging to apply in structuring or producing items for daily life; especially the wear resistance of small-scaled pillar structures may be poor.[48,109,110] Quick, cheap and relatively easy techniques to fabricate robust surfaces are required wholly to exploit the potential of structures for hydrophobic and water-directing surfaces. As numerous studies[2,4,6,16,17,19,20,22,28,33,34,43-55,59-61] have shown, hierarchical structures are required to achieve superhydrophobicity, but surfaces with micro-scale structures alone[83,88-89] have potential in the creation of anisotropic surfaces.

1.3 AIMS OF THE STUDY

The overall aim of this work was to study and develop relatively easy, quick and reproducible methods for structuring polymer. Polypropylene (PP) was chosen as the model surface material. Answers to the following questions were sought:

- How can isotropic and anisotropic microdepression patterns on mould inserts be created and transferred to polypropylene as pillar structures, and is it possible to combine nanoprotrusions with micropillars?
- As compared with micro-scale structures, how do the hierarchical structures affect wettability?
- Are there differences in the hydrophobic properties of anisotropic surfaces according to the orientation of their structures?
- Is there an easy way to create micropillar-structured moulds for micropit-structured polypropylene, and is it possible to fabricate hierarchical structures where micropits are covered with nanopits?
- How do pit structures affect the hydrophobicity of polypropylene?

The experimental work of this thesis is described in the following three chapters. Chapter 2 describes the fabrication processes and fabricated surface types, Chapter 3 the evaluation of fabrication methods and Chapter 4 the effects of surface structures on the behaviour of water. Finally, Chapter 5 summarizes the conclusions of the thesis.

2 STRUCTURING OF POLYPROPYLENE

Pillar- and pit-structured polypropylene surfaces, with and without nanostructure, were fabricated by injection moulding. The moulding of each structure required the preparation of a mould insert with complementary structure.

2.1 FABRICATION PROCESS

Mould inserts were fabricated through the microstructuring of aluminium (Al) foils (Alfa Aesar Puratronic®, 99.997% Al, thickness 0.25 mm). Before microstructuring, the Al foils (sized 3.3 cm * 4.2 cm or 3 cm * 3.5 cm) were degreased by keeping them 10 min in acetone in an ultrasonic bath at room temperature. The degreasing was followed by electropolishing in a mixture of perchloric acid and ethanol (1:8). Platinum foil was used as a counter electrode, the current was 2.7 A and time was 135 s. Polished foils were rinsed with deionised water and allowed to dry at room temperature.

Microstructuring of the Al foils was done with a micro-working robot RP-1AH from Mitsubishi Electric. The robot operated with a CR1 control unit and a feedback unit from Delta Enterprise Ltd. Tungsten carbide needles were supplied by Gritech Ltd. The working parameters of the robot and the processing steps after micro-working were varied according to the type of surface for which the insert was fabricated (see Figure 2). Processing steps are discussed in detail in Section 2.2.

PP surfaces were fabricated by injection moulding with the prepared mould inserts. PP was polypropylene homopolymer, HD 120 MO, density 908 kg/m^3 from Borealis Polymers Ltd. The moulding was done with a DSM Midi 2000 extruder and microinjection moulding machine. The processing parameters were screw temperature 255 °C, screw rotation speed 100 rpm, injection temperature 230 °C, mould temperature 50 °C–90 °C and air pressure of injection piston 4.0 or 5.0 bar. The moulded polymer pieces were circular discs, diameter 25 mm, with the structured area on one side and the other side smooth.

2.2 TYPES OF FABRICATED SURFACE

The fabricated surfaces can be divided into four classes according to their patterning and the fabrication process: isotropic pillars, anisotropic stripe-like pillars, anisotropic zone-like pillars and isotropic pits. The main steps in the fabrication of the different surface types are set out in Figure 2 and described in the text below.

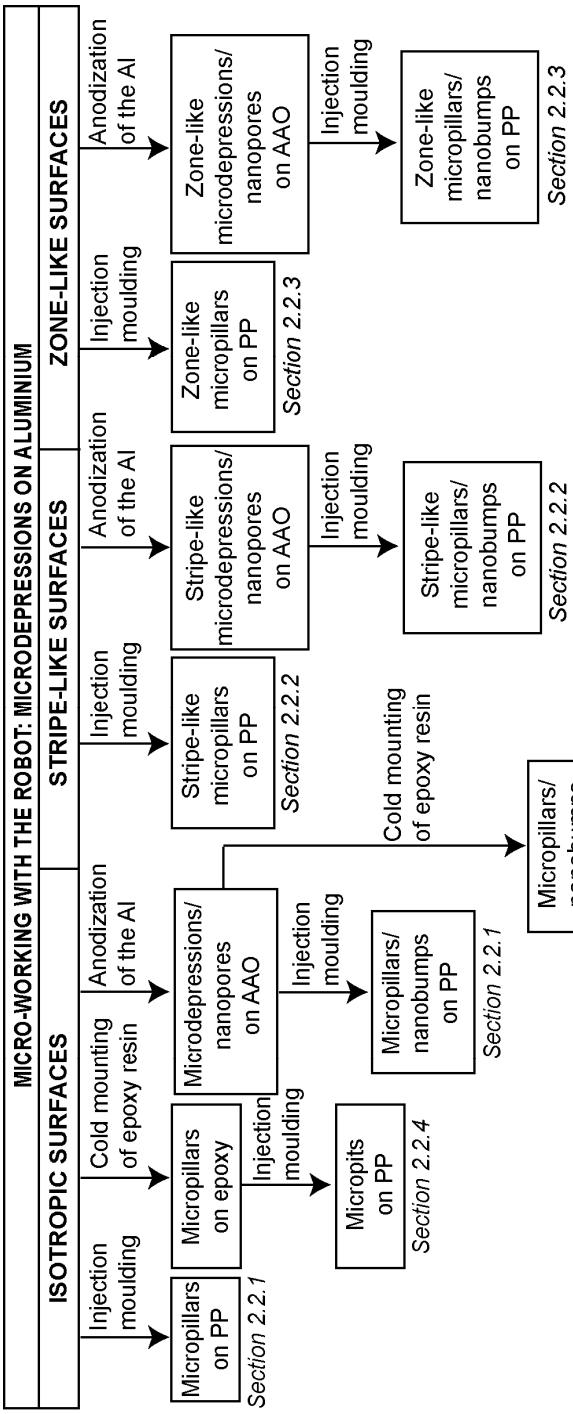

Figure 2. Scheme showing types of fabricated surface and main steps in their preparation.

2.2.1 ISOTROPIC PILLAR SURFACES

Six isotropic micropillar surfaces and four isotropic micropillar/nanobump surfaces were fabricated (Publication 1). Table 1 shows the fabricated Al structures for mould inserts. “Step” is a working parameter of the robot and is measured as the distance between two adjacent depressions. The structured area was 1 cm * 1 cm. The Al structures designated as “micro” were cut into circular discs, 25 mm in diameter, and used as mould inserts for injection moulding. The Al structures designated as “dual” were anodized after micro-working to obtain nanopores.

Table 1. Aluminium structures for isotropic pillar surfaces.

Structure	Step (µm)	Type
µ1	22	Dual
µ2	25	Micro + dual
µ3	40	Dual
µ4	25	Micro
µ5	30	Micro
µ6	40	Micro + dual
µ7	45	Micro
µ8	45	Micro

The anodization process was based on a previous research with some modifications[21]. The back-side of the structured aluminium foil was protected against anodization with nail polish (Maybelline Foreverstrong + Iron). Anodization was carried out at a constant voltage (40 V) in 0.3 M $C_2H_2O_4$ at 3 °C for 48 h using platinum foil as a counter electrode. After anodization the protective nail polish was removed with acetone. The native oxide layer from the aluminium surface was removed with 5 M NaOH, after which the unreacted aluminium was removed with 0.5 M $CuCl_2$. The removal was facilitated by adding two or three drops of 37 % HCl. The barrier layer was removed with 5 % H_3PO_4 solution at 30 °C for 40 min. After cutting into discs the anodized foils were glued onto 0.5-mm-thick steel plates with heat-stable epoxy glue (Loctite® Hysol® 9492 A&B), the anodized side facing upwards, and used as mould inserts. Mould temperature during the injection moulding was 50 °C.

2.2.2 ANISOTROPIC STRIPE-LIKE PILLAR SURFACES

Eighteen anisotropic stripe-like surfaces were fabricated, where pillar zones with one or three rows of micropillars alternated with smooth zones. Nine of the surfaces were further furnished with nanostructure on both pillar and smooth zones. Anisotropy stemmed from the stripe-like arrangement of zones: the structures appeared different when viewed parallel and perpendicular to the zones. Figure 3 shows the parameters of stripe-like structures and explains the two viewing directions.

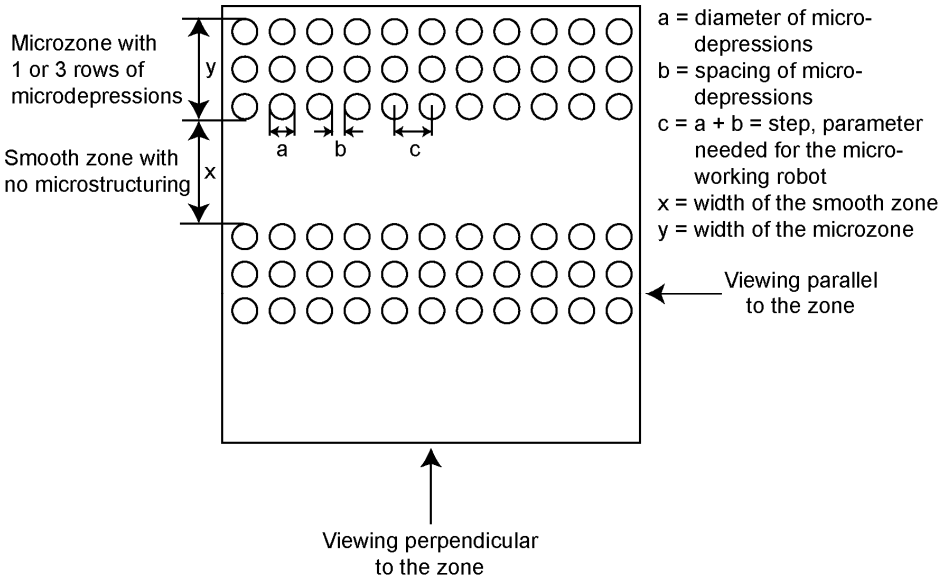

Figure 3. Stripe-like microstructure on aluminium foils for injection moulding.

The widths of the smooth and structured zones and steps between the micropillars were varied. The microstructured area was 0.7 cm * 1 cm and the number of created zones was dependent on the widths of the zones. The dimensions of the microstructures were controlled with the working parameters of the micro-working robot.

Nine different microstructures were fabricated, each on two Al foils. One of the two microstructured foils was cut as a circular disc, 25 mm in diameter, and used as a mould insert. The other was anodized to obtain an AAO foil with microdepressions and nanopores. The anodization was done as for the isotropic structures (Section 2.2.1) except that the anodization time was 24 h. After gluing the AAO foil onto a steel plate, the foil was used as a mould insert. Injection pressures of 4.0 bar and 5.0 bar and mould temperatures 50 °C, 60 °C, 70 °C, 80 °C and 90 °C were tested. The parameters of each foil are presented in Table 2.

Table 2. Main parameters for the anisotropic stripe-like aluminium and anodized aluminium oxide structures. "W" means width.

Structure	Step (µm)	Rows of depressions in microzone	W. of micro-zone (µm)	W. of unstructured zone (µm)
1-Row microstructures				
µ8	25	1	15	75
µ12	25	1	15	60
µ14	25	1	15	205
1-Row micro/nanostructures				
µ7+n	25	1	15	75
µ11+n	25	1	15	60
µ13+n	25	1	15	205
3-Row microstructures				
µ2	25	3	65	130
µ4	25	3	65	65
µ6	40	3	100	200
µ10	40	3	100	100
µ16	40	3	100	500
µ18	40	3	100	40
3-Row micro/nanostructures				
µ1+n	25	3	65	130
µ3+n	25	3	65	65
µ5+n	40	3	100	200
µ9+n	40	3	100	100
µ15+n	40	3	100	500
µ17+n	40	3	100	40

2.2.3 ANISOTROPIC ZONE-LIKE PILLAR SURFACES

Four types of zone-like surfaces (Publication IV) were created (see Figure 4). A common feature was that they consisted of three parallel zones where the edge zones were identical, consisting of micropillars or micropillars/nanobumps, and the middle zone differed. For each of the four types, the width of the middle zone was varied, for total of 31 different surfaces.

The microstructures for mould inserts were created as 1 cm * 1 cm or 0.5 cm * 0.5 cm areas of microdepressions, with microdepressions of constant diameter and constant spacing between. They were designed with a drawing program and converted to a specific file format for the micro-working robot. For the surface type with micropillars only, the structured Al foils were glued onto circular steel plates (diameter 25 mm) and used as mould inserts for injection moulding. For the three surface types with hierarchical micropillar/nanobump structures, the microstructured foils were anodized and the Al/AAO foils cut as circular discs (diameter 25 mm). The anodization was done basically as with stripe-like structures (Section 2.2.1), but the unreacted aluminium was

not removed. Instead, immediately after anodization the AAO foils were immersed in 5 % H_3PO_4 for 40 min to open the nanopores of AAO. The gluing onto circular steel plates was done as explained in section 2.2.1. During injection moulding, the air pressure of the injection piston was 5.0 bar and the mould temperature 70 °C.

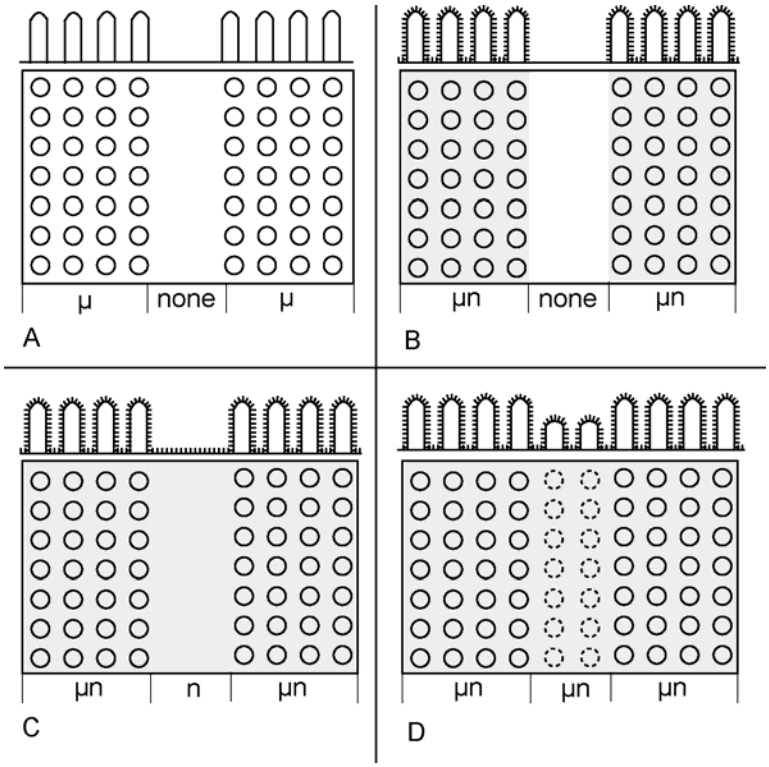

Figure 4. Anisotropic zone-like surfaces. **A.** Edge zones with micropillars and an unstructured middle zone. **B.** Edge zones with hierarchical micropillars/nanobumps and an unstructured middle zone. **C.** Edge zones with hierarchical micropillars/nanobumps and a middle zone with nanostructure. **D.** Edge zones with hierarchical micropillars/nanobumps and a middle zone with hierarchical micropillars/nanobumps where micropillar height differs from that in the edge zones.

2.2.4 ISOTROPIC PITTED SURFACES

Five isotropic micropit surfaces and three isotropic micropit/nanodepression surfaces (Publication III) were fabricated as 1 cm * 1 cm areas.

In fabrication of the mould inserts, the needle size and step parameter for the robot were varied to obtain microdepressions with different diameters and spacings. When a needle with diameter 15 μm – 20 μm was used, the step parameters were between 30

µm and 55 µm; with a 100-µm needle the step parameters were 125 µm – 150 µm. Three Al foils were anodized as described in Section 2.2.3 to obtain microdepression/nanopore -structured Al/AAO foils.

The microstructured Al foils and micro/nanostructured Al/AAO foils were used as moulds for the novel method of cold mounting of epoxy resin (SpeciFix Resin + Curing Agent 20 from Struers). Greased rubber rings were used as frames to surround the structured areas and hinder the spreading of the liquid epoxy. Steel plates and weights (21 – 28 g) were placed on the epoxy surface to assist the filling of the structures. Furthermore, since the steel plates adhered to the epoxy during hardening they also served as supports in subsequent processing steps. When the epoxy had hardened, the Al or Al/AAO foils were etched away with 5 M NaOH and 0.5 M $CuCl_2$ solutions to expose the micropillar- or micropillar/nanobump-structured epoxy surfaces. Supported by the steel plates, the epoxy surfaces could be used as mould inserts for injection moulding. The mould temperature was 50 °C and pressure 5.0 bar.

The epoxy mounting procedure is depicted in Figure 5.

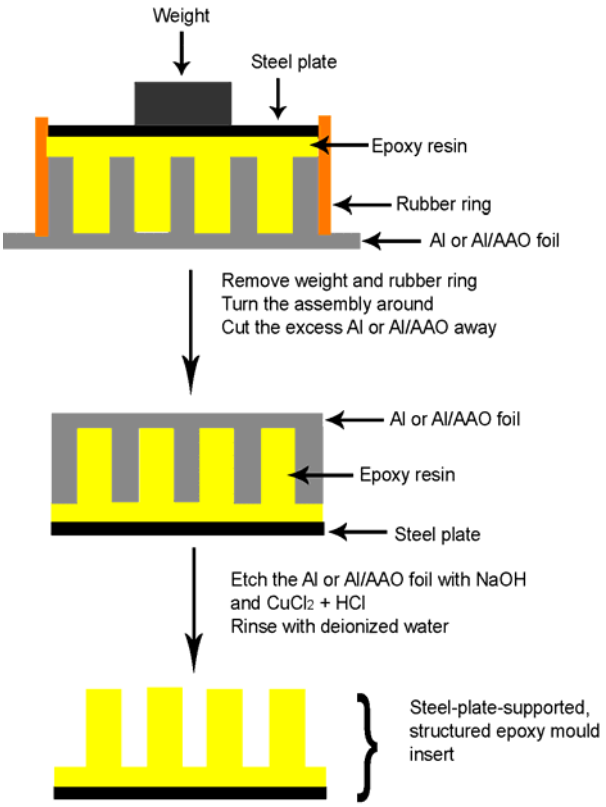

Figure 5. Fabrication of structured epoxy mould inserts. The scheme is not drawn to scale.

3 EVALUATION OF FABRICATION METHODS

The structures of the mould inserts and moulded PP surfaces were imaged by scanning electron microscopy (SEM). From the images, the average dimensions of the structures were measured to determine how the target parameters had been realised and how accurately the planned structures had been copied on the PP. For the epoxy mould inserts and pit-structured PP surfaces, the proportions of defects were estimated as well. Most of the mould inserts were imaged before and after injection moulding to see if they were damaged during the moulding process.

For evaluation of the methods, the surfaces are divided into three groups: micropillar-, micropillar/nanobump-, and micropit- and micropit/nanodepression-structured surfaces.

3.1 PERFORMANCE OF THE ROBOT IN MICRO-WORKING

The structuring of aluminium with a micro-working robot offered a reliable and easy way to fabricate Al foils with microdepressions for use as mould inserts. The accuracy of the robot in reproducing the step between the depressions was good. The diameters of the depressions depended of the profile of the needle: the bottom of depression was as wide as the tip of the needle, while the mouth was as wide as the diameter of the needle at working depth. Because the sides of the needles were not perfectly smooth on microscale, irregular structures stemming from the needles were formed on the walls of the microdepressions.

The depth parameter of the robot was a relative value, depending on the contact between the needle and aluminium. Real depths of the depressions were not measured because this could not be done without destroying the Al foils.

The control program of the robot allowed planning of simple, rectangular areas where step and depth of depressions remained constant. With a drawing program it was possible to create complex areas with various depths and steps of depressions and with unstructured zones.

3.2 STRUCTURING OF POLYPROPYLENE SURFACES WITH MICROPILLARS

When the microstructured Al foils were used as mould inserts as such, some bending of the foil occurred during the detaching of the moulded PP discs. When the foil was glued onto a steel plate, the durability was good and detaching easy, and a number of PP discs could be moulded without damage to the insert. Only occasionally did the insert bend, become dented or disengage from the supporting steel plate.

The injection moulded PP structures, moulded with mould temperature 50 °C, were as planned, and the diameters and spacings of the micropillars corresponded with those of the mould inserts. Because of the low mould temperature, filling of deep holes was sometimes incomplete, leading to pillars of varying heights and with rounded tops. The air pressure of the injection piston (4.0 or 5.0 bar) did not have a notable effect on replication accuracy.

3.3 STRUCTURING OF POLYPROPYLENE SURFACES WITH MICROPILLARS/NANOBUMPS

During the anodization process, the microdepressions on Al foils became deeper and wider, making the dimensions of the micropillars in PP more difficult to predict, and there was more variation. The diameters of the nanopores formed during anodization were dependent on the anodization voltage, and the depths were dependent on the anodization time. The treatment with phosphoric acid after anodization also had an effect on the pore size, making the pores wider and their walls thinner. When the anodization and post-anodization conditions were the same for different Al foils, their nanostructures were of approximately the same dimensions.

Usually when nanostructured AAO foils have been used as moulds for structuring polymers (e.g., Ref. 21 and 22), the side with regular nanostructure has been facing upwards in the moulding. This regular structure is formed by the bottoms of the nanopores when growing into the Al foil. The regular structure is exposed by removing the unreacted aluminium[21-22]. When the Al foil is furnished with microstructures, however, these appear on the upward face as bumps, not as depressions. Because in this work it was desired that the mould insert should have structure with microdepressions and nanopores, the only alternative was to use the “downside” of the AAO with irregularly arranged nanopores. This option also had an advantage: the fabrication of the mould insert is simpler because the unreacted aluminium does not need to be removed. After anodization the only necessary post-treatment is to immerse the Al/AAO foil in phosphoric acid for 40 min to open the nanopores.

The method of preparing inserts used in studies I and II was slightly more complex than that just described, as it included the removal of the unreacted aluminium from anodized Al/AAO foil and gluing of the remaining AAO foil onto a steel plate. This method was somewhat time-consuming and requiring of care because after the removal of aluminium the AAO foil was very fragile. The gluing onto steel had to be done carefully, and even then there were occasions on which the AAO foil broke during the moulding.

In study IV the aluminium was not removed. After anodization Al/AAO foils were treated with phosphoric acid, cutted as circular discs and used as mould inserts. The durability of these Al/AAO inserts was good and they were easily detached from the PP discs.

The mould temperature had an effect on the replication accuracy of PP. With too low mould temperature the microholes of the mould insert were not completely filled, which could be seen as rounded and smooth micropillar tops and varying pillar diameters. If the temperature was too high, the polypropylene stuck to the insert during detaching and the micropillars bent and broke. Mould temperature of 70 °C gave the best replication accuracy during the moulding. If the micropillars were very high (microdepressions in the insert were deep), the replication of the nanostructures on micropillar tops was inadequate or there was no nanostructure at all. With shallower microdepressions also the pores on the bottoms were filled during the injection moulding, and low micropillars with nanobumps or nanohairs on tops were formed. The sides of pillars and areas between the pillars were well covered with bumpy or hairy nanostructure, independent of the micropillar height or mould temperature. Figure 6 shows examples of different structure scales on mould insert and PP moulded at 70 °C.

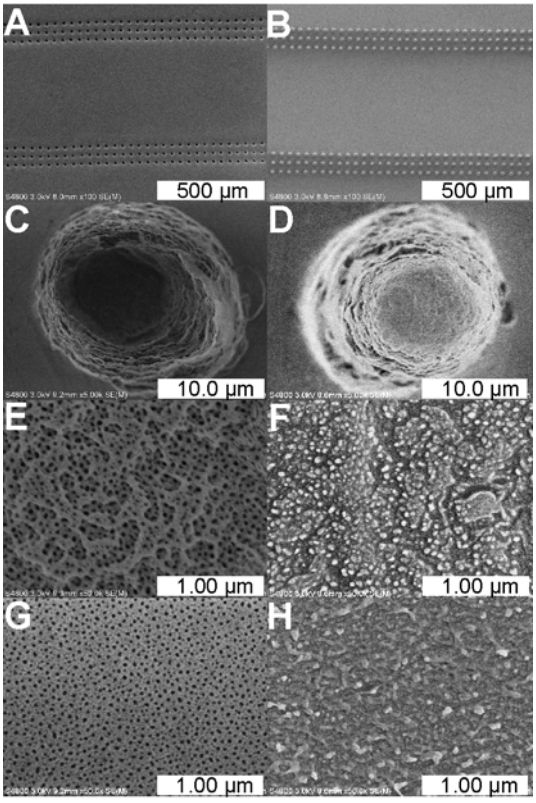

Figure 6. On left, SEM images of an anisotropic stripe-like AAO mould insert with microdepressions and nanopores, and on right, a PP sample moulded with the insert. **A. and B.** Stripe-like arrangement of microstructures. **C. and D.** A microdepression and a micropillar. **E. and F.** Nanopores on bottom of a microdepression and nanobumps on top of a micropillar. **G. and H.** Nanopores and nanobumps on a smooth zone.

The effect of moulding temperature on the replication accuracy can be exploited to control the occurrence of the different structure scales. With lower mould temperature it is possible to fabricate micropillar surfaces where the smooth areas between pillars and the lower parts of micropillar walls are covered with nanostructures while the micropillar tops are without structure.

3.4 STRUCTURING OF POLYPROPYLENE SURFACES WITH MICROPITS AND MICROPITS/NANODEPRESSIONS

Obtaining micropit- and micropit/nanodepression structures by injection moulding required mould inserts with compelementary micropillar- and micropillar/nanobump structures. Micro- and micro/nano-structured foils were used as moulds for cold mounting of epoxy resin. With the developed mounting process, epoxy discs with micropillars or micropillars/nanobumps were prepared.

Filling of the mould structures and replication accuracies in epoxy were good, although the structural parameters on the epoxy discs were not exactly the same as those on the Al foils. The diameters of the epoxy pillars differed somewhat from the complementary diameters of the microdepressions on Al, and there was more variation in the pillar diameters than the depression diameters. Nanostructures were seen as low bumps completely covering the micropillars and areas between them.

There were some defects, such as missing or broken pillars, on the epoxy surfaces. The original foils had to be removed from the hardened epoxy by etching and this and the washing of the epoxy surfaces that followed the etching may have harmed the structures. Occasionally there were defects originating from air pockets or air bubbles formed in the microdepressions during the cold mounting. However, the quality of the epoxy discs was still good enough that they could be used as mould inserts for injection moulding. The pressure used was 5.0 bar and mould temperature 50 °C. Higher mould temperature (70 °C) was also tested, but it had no effect on the replication accuracy.

The durability of the epoxy mould inserts was good and they were easy to detach from polypropylene discs when the micropillars were relatively thick (diameter ~30 μm or greater). When the micropillars were thinner than 30 μm, PP tended to stick on the insert and the insert structure was damaged. The thicker micropillars replicated with good quality as micropits on PP, with diameters slightly greater than on the original Al foils. As with the diameters of the epoxy micropillars, the diameters of the micropits on PP varied slightly more than the microdepressions on Al. When there were nanobumps covering the pillars on epoxy, they were replicated on as shallow nanodepressions covering the walls and bottoms of the micropits and the areas in between. To fully exploit the effects of nanostructures, it might be better if they were deeper: pits instead of depressions. Nevertheless, the nanodepressions were distinct enough to show that hierar-

chical pit-like micro/nanostructures were achieved. Figure 7 shows examples of structures on Al/AAO, on epoxy mould insert and on moulded PP.

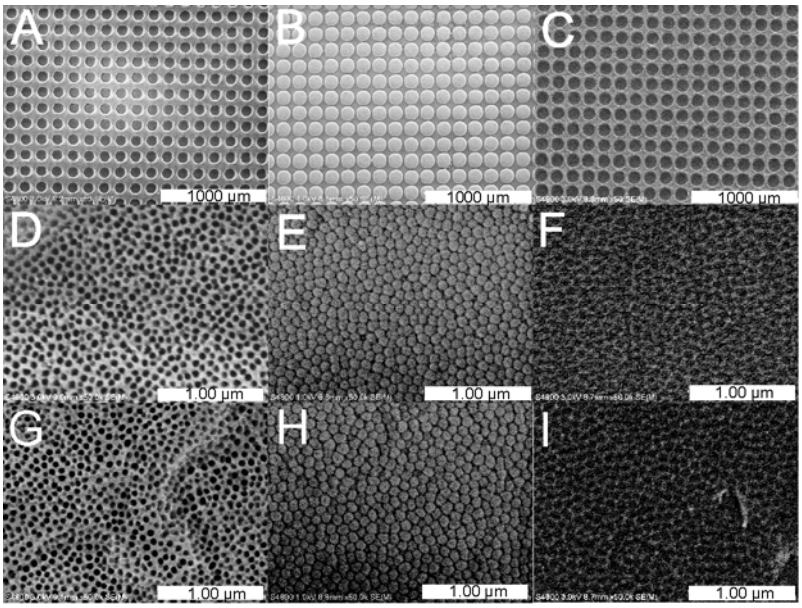

Figure 7. Sructures on Al/AAO, on epoxy and on PP. **A., D. and G.** Microdepressions on Al/AAO and nanopores between and on the bottom of microdepressions. **B., E. and H.** Micropillars on epoxy and nanobumps between and on top of micropillars. **C., F. and I.** Micropits on PP and nanodepressions between and on bottom of micropits.

4 EFFECT OF SURFACE STRUCTURES ON CONTACT AND SLIDING ANGLES OF WATER

Hydrophobic properties of fabricated surfaces were analyzed by measuring static and dynamic contact angles and sliding angles. Measurements were carried out with a KSV Cam 200 contact angle meter using room-temperature deionised water. Six to nine parallel discs were used for each structure. When the structured area was 0.5 cm * 0.5 cm, there was just one measurement point, with the droplet placed at the centre. When the area was larger (1 cm * 0.7 cm or 1 cm * 1 cm), there were three measurement points; on homogenous and stripe-like surfaces the three points were located around the centre, and on zone-like surfaces one measurement point was at the centre of the middle zone and other two at the centres of the edge zones.

For the discussion of structural effects, surfaces are divided into the same three groups as in Chapter 3.

4.1 MEASUREMENT OF CONTACT AND SLIDING ANGLES

For static contact angle measurements (publications I-III), a droplet of water (5 or 6 µl) was placed at the measurement point and photographed once a second for 30 seconds (see Figure 8A). The Young-Laplace equation was then fitted to the profile of the droplet. The average static contact angle was calculated from the values obtained between 5 and 30 s.

For dynamic contact angle measurements (publications III-IV), a droplet of water (2 µl) was placed at the measurement point and carefully expanded to 8 µl (see Figure 8B). During the expansion, the droplet was photographed 70 times at 120-ms intervals. Water was then removed, and as the droplet contracted it was photographed 140–210 times at 120-ms intervals until the shape became distorted or the droplet detached from the surface. The Young-Laplace equation was fitted to the profile of the droplet and the contact angles during the expansion-contraction process were plotted as a function of the volume of the droplet. With the help of the plots, the regions for advancing and receding angles (the regions where the contact angle did not substantially change but the droplet expanded or contracted) were defined, and average advancing and receding angles were calculated. The advancing region was from about 3 to 7 µl and the receding region from 7 to 3 µl.

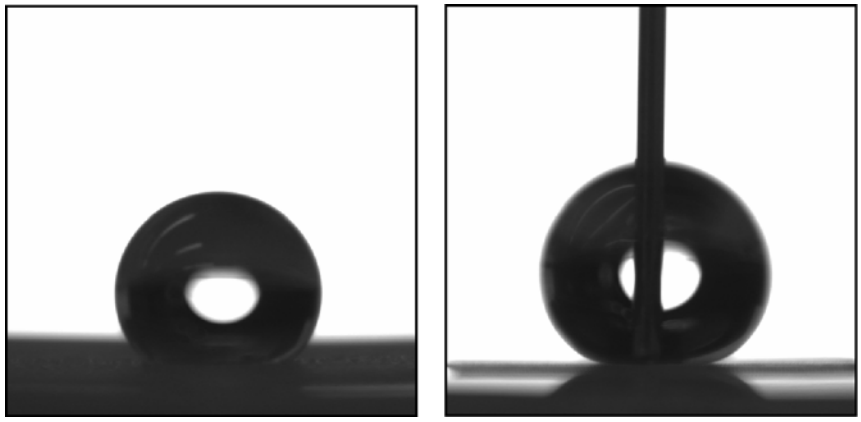

A B

Figure 8. Examples of droplets during the measurement of contact angles. **A.** A droplet on a surface during the measurement of static contact angles. **B.** A droplet on a surface during the measurement of dynamic contact angles.

For sliding angle measurements, in study I a droplet of water (6 µl) was dropped onto the tilted surface from about 1 mm height. The tilt of the surface was increased, and the reported value was the value of the tilting angle when the droplet began to roll on the surface. In studies II and IV a droplet of water (6 µl) was placed on the disc and the measurement bench was tilted until the droplet began to roll. Photographing com-

menced simultaneously with the tilting of the bench. Values reported for the sliding angles were the tilt angles of the bench at which the droplets began to roll.

The contact angles reported in Publications I and II cannot be straightforwardly compared with those reported in Publications III and IV, because of the difference in measuring techniques: static contact angles give values of metastabile states, whereas dynamic values give advancing and receding angles representing the highest and lowest possible values[56]. Both techniques also have their own sources of error. It has also been questioned if the more conventional static drop method is not the best way to describe the hydrophobicity of surfaces[48,62,63]. There are arguments that dynamic angles would be more informative because they are not dependent on the way the droplet is placed on the surface[48,56,58,62,63].

Moreover, since research groups use different drop sizes, equipment and calculation methods, comparisons of absolute contact angle values between groups need to be done with caution[11,41,47]. Trends in the measured values should, however, be comparable and can be used to evaluate the effects of structure types and dimensions on hydrophobic properties of surfaces[47].

Calculations of theoretical contact angles and comparisons between them and the measured values were done only in the cases of homogeneous (Publication I) and stripe-like (Publication II) surfaces. In these calculations, there were some complications and weaknesses. The dimensions of the structures varied somewhat over the areas and were hard to estimate properly. Also the calculations of roughness factors and area fractions are dependent of the selected theoretical model (contact line or contact area model) for contact angles, and it is not clear which model is the best[16,43,50,78-82]. In any case, all the models are simplifications of the real surfaces. It did not seem very meaningful to concentrate on the extensive theoretical calculations, because the main concern during studies I-IV was to develop effective methods for fabricating different structures that could be used for controlling the movement of water on polypropylene.

4.2 POLYPROPYLENE SURFACES STRUCTURED WITH MICROPILLARS

Isotropically and anisotropically arranged micropillars had different effects on the behaviour of water. Also, properties were slightly different with the different types of anisotropy.

Isotropic micropillar surfaces

With properly chosen microstructure parameters, near-superhydrophobic surfaces were achieved on isotropic micropillar surfaces (Publication I). Measured contact angles were ~150° and sliding angles ~10°. Theoretical Wenzel and Cassie-Baxter contact

angles were calculated and compared with the experimental values. When surfaces were near-superhydrophobic, the experimental contact angles followed the Cassie-Baxter values, showing that on these surfaces the droplets rested on the composite surface formed by the micropillar tops and the air between. If the micropillars were not high enough or the spacings were too wide, the water droplets migrated down the pillar walls and contacted the surface between the pillars. The experimental contact angles were then in line with Wenzel values.

Stripe-like micropillar surfaces

On stripe-like micropillar surfaces (Publication II), with alternating micropillar (one or three rows) and smooth (without micropillars) zones (see Figures 3 and 9), behaviour of the droplets was clearly direction-dependent. All surfaces were hydrophobic, some of them even superhydrophobic, when viewed parallel to the zones. Viewed perpendicularly, the contact angles were noticeably lower when the smooth zones were widened, and superhydrophobicity was achieved only with narrow smooth zones. Neither viewing direction nor zone width had a clear effect on sliding angles: they were 7°–8° on 1-row structures and 9°–15° on 3-row structures. Table 3 and Figure 10 show the static contact angles on stripe-like micropillar surfaces where the micropillar stripes consisted of one or three rows of microstructures, and the three-rowed structures were fabricated with narrow and wide spacing between the pillars.

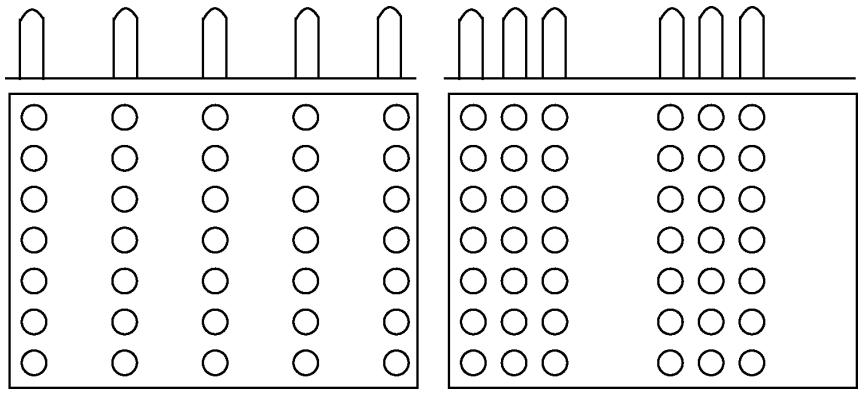

Figure 9. Schemes of stripe-like surfaces with alternating micropillar and smooth zones. **A.** A 1-row microstructure. **B.** A 3-row microstructure.

The theoretical Wenzel and Cassie-Baxter values for anisotropic surfaces are complicated to calculate and there is some evidence that they may not be applicable at all, especially for dynamic angles[47]. Some calculations were made for stripe-like structures, and on the basis of comparisons between calculated and static values and observations

during the contact angle measurements, it was concluded that the droplets adopted a metastabile Cassie-Baxter state, just as droplets do on lotus leaves[53].

Table 3. Measured contact angles and their standard deviations on microstructured stripe-like polypropylene surfaces. "W" means width and "para" and "perp" refer to parallel and perpendicular viewing.

Structure	Step (µm)	W. of the unstructured zone (µm)	CA para	CA perp
1-Row microstructures				
µ12	25	60	162 ± 3	157 ± 13
µ8	25	80	163 ± 4	158 ± 10
µ14	25	200	142 ± 11	111 ± 19
3-Row microstructures with narrow spacing				
µ4	25	65	146 ± 12	123 ± 20
µ2	25	115	147 ± 14	127 ± 24
3-Row microstructures with wide spacing				
µ18	40	35	161 ± 3	159 ± 2
µ10	40	95	165 ± 5	160 ± 9
µ6	40	190	119 ± 11	104 ± 3
µ16	40	495	113 ± 9	105 ± 2

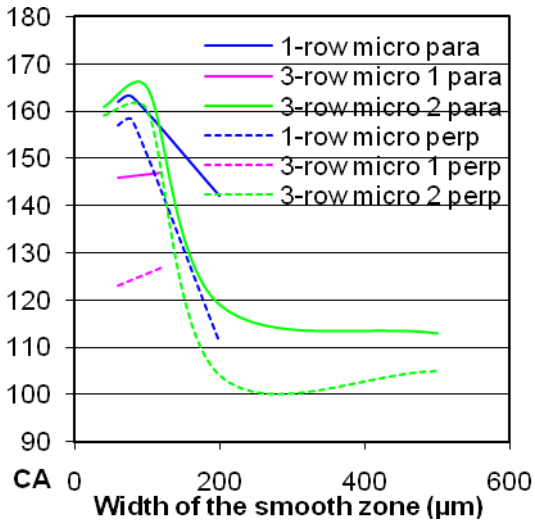

Figure 10. Contact angles on stripe-like micropillar surfaces. "para" and "perp" refer to contact angles measured parallel and perpendicular to the microstructure stripes, and the preceding numbers 1 and 2 refer, respectively, to narrow and wide spacing between the pillars.

Zone-like micropillar surfaces

On zone-like surfaces (Publication IV) the unstructured middle zones were wider than the smooth zones on stripe-like surfaces (see Figures 4A and 11). Surfaces were clearly hydrophobic, but superhydrophobicity was not achieved. The differences between viewing directions were clear. When the unstructured zone was widened, the droplets sank deeper in between the micropillar zones, and contact angles became lower in parallel and slightly higher in perpendicular viewing direction: at the same time the hysteresis decreased. The droplets became distorted from their original spherical shape because they elongated parallel to the unstructured zone even though they remained perched on the micropillars edging the unstructured zone. When the zone was wide enough that the droplets fell to the bottom, they spread along the smooth middle zone, unable to penetrate between the adjacent micropillars. Because they tended to assume the spherical shape, differences between viewing directions were reduced. Figure 11 presents a cross-section and a view from above of a zone-like micropillar surface.

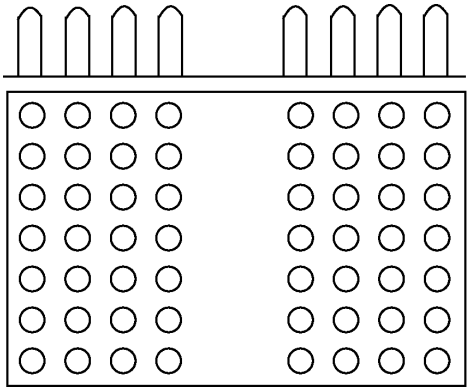

Figure 11. A scheme of a micropillar-structured polypropylene surface with an unstructured middle zone.

Table 4 and Figure 12 show the values of advancing and receding contact angles for zone-like microstructures with an unstructured middle zone with increasing width. Two sets of values are given for middle zone width of 0 μm, because they were estimated with two sets of parallel samples: the other set was fabricated together with zone widths of 1200 μm, 1290 μm and 1430 μm, and the other with zone widths of 1620 μm, 1900 μm and 2160 μm. Also the hysteresis values are presented in Table 4. Theoretical contact angle values were not calculated.

Table 4. Advancing and receding contact angles and their hystereses for micropillar-structured polypropylene surfaces with an unstructured middle zone.

Width of the middle zone (µm)	Parallel viewing of contact angles			Perpendicular viewing of contact angles		
	Advan-cing	Reced-ing	Hyster-esis	Advan-cing	Rece-ding	Hyster-esis
0	148 ± 9	129 ± 11	19 ± 6	145 ± 7	127 ± 9	19 ± 3
1200	151 ± 6	134 ± 6	17 ± 4	101 ± 4	83 ± 5	18 ± 3
1290	152 ± 4	136 ± 6	16 ± 4	102 ± 2	88 ± 4	14 ± 2
1430	147 ± 4	131 ± 5	16 ± 3	99 ± 6	86 ± 8	13 ± 2
0	156 ± 6	146 ± 3	10 ± 4	159 ± 9	143 ± 4	16 ± 7
1620	146 ± 4	141 ± 6	5 ± 5	101 ± 2	87 ± 3	14 ± 3
1900	137 ± 2	130 ± 5	6 ± 5	102 ± 3	89 ± 2	13 ± 1
2160	124 ± 3	119 ± 7	6 ± 6	104 ± 1	91 ± 2	13 ± 2

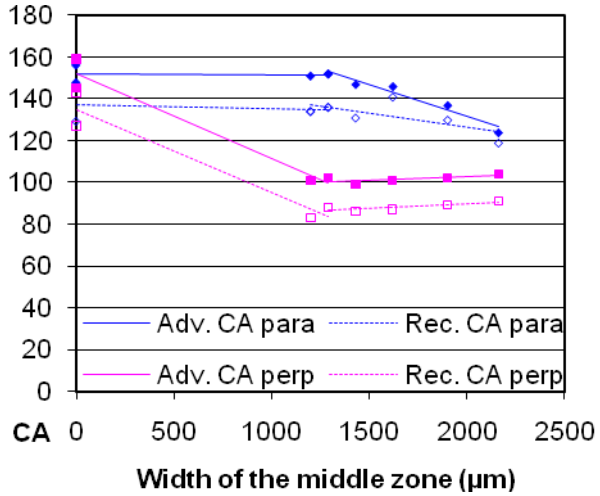

Figure 12. Advancing and receding contact angles for micropillar-structured polypropylene surfaces with an unstructured middle zone. "para" and "perp" refer to contact angles measured parallel and perpendicular to microstructure zones.

4.3 POLYPROPYLENE SURFACES STRUCTURED WITH MICROPILLARS/NANOBUMPS

As with the single structures, also with the hierarchical structures there were differences in the hydrophobic properties of isotropic, stripe-like and zone-like surfaces.

Isotropic micropillar/nanobump surfaces

Isotropic hierarchical surfaces (Publication I) showed superhydrophobicity, with static contact angles over 150° and sliding angles ~10° or lower. On one surface, an average static contact angle of 164° and a sliding angle of ~2.5° were achieved. Comparison of theoretical and experimental values showed that, on hierarchical structures, the droplets adopted Cassie-Baxter state: nanostructure increased the area of the composite interface and the droplets more easily adhered to the micropillar tops.

Stripe-like micropillar/nanobump surfaces

On anisotropic stripe-like surfaces (Publication II) (see Figure 13), nanostructure clearly helped to achieve the superhydrophobic state, increasing contact angles even when the nanostructure on micropillars was incomplete. On these surfaces the smooth zones (without micropillars) were covered with hairy and bumpy nanostructures, which also supported the droplets.

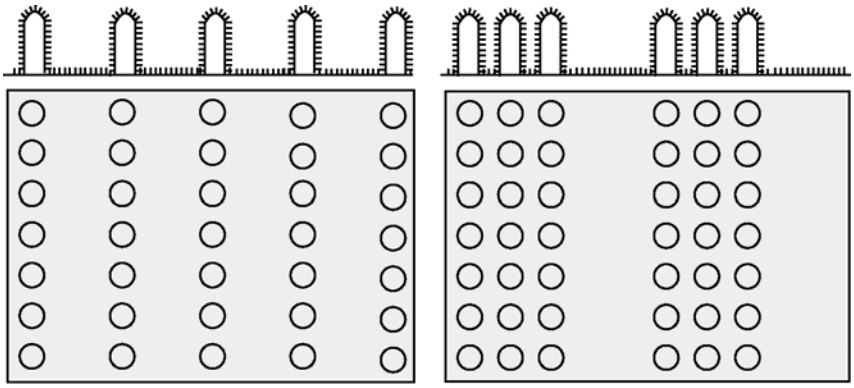

A. B.

Figure 13. Schemes of stripe-like surfaces with alternating micropillar/nanobump and nanobump zones. **A.** A 1-row micro/nanostructure. **B.** A 3-row micro/nanostructure.

The static contact angles and sliding angles showed superhydrophobicity in both viewing directions, and during the measurements the droplets adopted the Cassie-Baxter state. The calculated theoretical Cassie-Baxter values were in line with the experimental results. Table 5 and Figure 14 present the static contact angles on stripe-like surfaces with one and three rows of micropillars moulded at mould temperature 50 °C.

The heights of the micropillars did not correlate with the contact angles: when the droplets were in the Cassie-Baxter state, they remained attached to the tops of the micropillars; the height of the micropillars was meaningless. Because of the supporting effect of the nanostructures, widening of the smooth zones did not result in lower con-

tact angles. The contact angle values remained almost constant, while the anisotropic effect was lessened. Still, surfaces were achieved that were both superhydrophobic and anisotropic, with static contact angles near 170° and sliding angles near 0°.

Table 5. Measured contact angles and their standard deviations on micro/nano-structured stripe-like polypropylene surfaces. "W" means width and "para" and "perp" refer to parallel and perpendicular viewing.

Structure	Step (µm)	W. of the unstructured zone (µm)	CA para	CA perp
1-Row micro/nanostructures				
µ11+n	25	60	166 ± 3	163 ± 2
µ7+n	25	75	162 ± 4	166 ± 4
µ13+n	25	200	160 ± 8	162 ± 8
3-Row micro/nanostructures with narrow spacing				
µ3+n	25	55	159 ± 8	156 ± 9
µ1+n	25	115	165 ± 4	161 ± 3
3-Row micro/nanostructures with wide spacing				
µ17+n	40	35	149 ± 5	154 ± 6
µ9+n	40	100	161 ± 5	161 ± 7
µ5+n	40	190	161 ± 6	150 ± 9
µ15+n	40	500	165 ± 5	155 ± 10

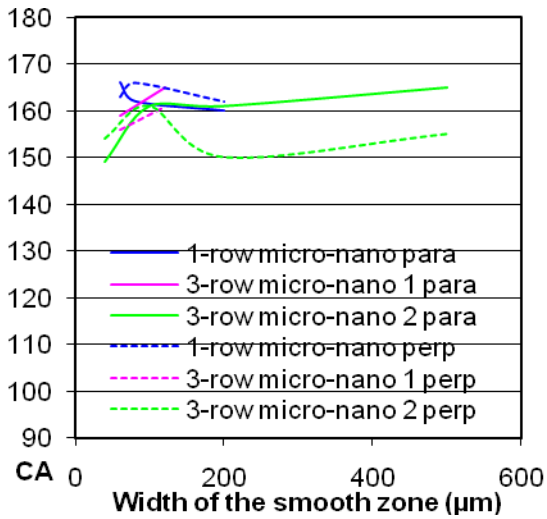

Figure 14. Contact angles on stripe-like micropillar/nanobump structures. "para" and "perp" refer to contact angles measured parallel and perpendicular to microstructure stripes, and the preceding numbers 1 and 2 refer, respectively, to narrow and wide spacing between the pillars.

Zone-like micropillar/nanobump surfaces

No true superhydrophobic state was achieved on zone-like surfaces (Publication IV) (see Figures 4B, 4C, 4D and 15): all the receding contact angles were less than 150°, although some advancing values were over 160°. Also, the sliding angles were not low enough for superhydrophobicity.

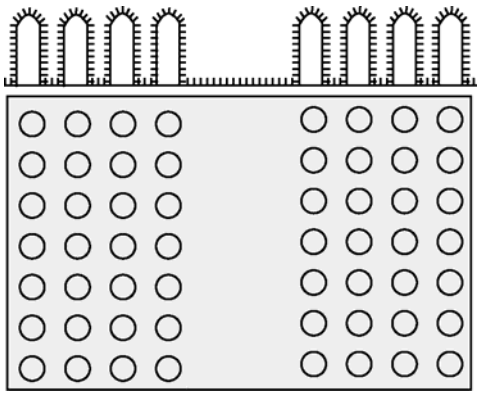

Figure 15. A scheme of a micropillar/nanobump-structured polypropylene surface with a nanostructured middle zone.

When the edge zones had hierarchical structures and the middle zone was unstructured (see Figure 4B), droplets behaved as expected. On the edge zones dynamic and sliding angle values were similar to those of reference isotropic hierarchical structures of the same study. Values for the unstructured middle zone were similar to those on smooth polypropylene. A 2200-µm-wide middle zone was wide enough that the droplets rested completely on the bottom, but even so the droplets elongated in parallel with the zone and there was anisotropy of contact angles.

With hierarchically structured edge zones and nanostructured relatively narrow middle zones (Figure 15), droplets behaved as if the surfaces were isotropic. When the mould temperature was 50 °C and nanostructure on upper parts of micropillars was lacking, widening of the middle zone resulted in lower contact angles, because the supporting effect of the nanostructure was less and the droplets began to sag into the middle zone. Still, even the widest zones were not so wide that the droplets sank totally to the bottom; they adhered at least partially to the micropillars and maintained their almost symmetrical shape, with no notable anisotropy. Table 6 shows the measured advancing and receding contact angles and their hystereses, and Figure 16 displays the measured contact angle values.

With mould temperature of 70 °C, the micropillar tops were always at least partially covered with nanostructures that supported the droplets. With moderate middle zone widths, the droplets “climbed” with the help of the nanostructures onto the micropillars.

When the middle zone became too wide for that, the nanostructure on the bottom still supported the droplets. In both cases, the droplets maintained their symmetrical shapes and there was no marked anisotropy of contact angles. Sliding angles increased when the middle zone was widened. Easy sliding of the droplets requires that they are well supported by both structure scales. Table 6 shows the measured advancing and receding contact angles and their hystereses, and Figure 17 shows the measured contact angle values.

Table 6. Advancing and receding contact angles and their hystereses for micropillar/nanobump-structured polypropylene surfaces with a middle zone with only nanostructure.

Width of the middle zone (μm)	Parallel viewing of contact angles			Perpendicular viewing of contact angles		
	Advancing	Receding	Hysteresis	Advancing	Receding	Hysteresis
Mould temperature 50 °C						
0	154 ± 7	142 ± 5	13 ± 6	150 ± 7	138 ± 5	11 ± 6
215	160 ± 5	142 ± 3	17 ± 4	154 ± 7	139 ± 6	15 ± 6
305	154 ± 7	147 ± 4	7 ± 3	157 ± 5	148 ± 6	9 ± 5
420	157 ± 4	142 ± 2	14 ± 3	149 ± 4	131 ± 10	19 ± 8
540	153 ± 4	136 ± 3	17 ± 4	146 ± 3	121 ± 8	25 ± 10
645	155 ± 7	143 ± 4	12 ± 5	149 ± 9	136 ± 7	12 ± 4
740	149 ± 10	132 ± 8	18 ± 4	138 ± 10	114 ± 9	24 ± 9
880	154 ± 3	142 ± 3	12 ± 2	151 ± 8	128 ± 7	23 ± 6
990	139 ± 16	132 ± 11	12 ± 9	133 ± 8	118 ± 12	17 ± 14
1090	146 ± 6	133 ± 5	13 ± 6	143 ± 8	121 ± 6	22 ± 10
Mould temperature 70 °C						
0	154 ± 6	140 ± 5	14 ± 6	151 ± 7	138 ± 6	15 ± 4
305	139 ± 13	131 ± 10	8 ± 6	143 ± 8	135 ± 5	8 ± 6
620	144 ± 10	136 ± 4	8 ± 10	136 ± 13	124 ± 7	12 ± 10
875	153 ± 8	142 ± 3	11 ± 8	145 ± 6	131 ± 7	14 ± 7
1075	146 ± 4	135 ± 4	11 ± 4	138 ± 3	127 ± 6	11 ± 5
1200	153 ± 8	138 ± 4	15 ± 10	142 ± 4	125 ± 9	17 ± 6
1300	153 ± 6	134 ± 7	19 ± 7	149 ± 3	126 ± 9	24 ± 8
1460	154 ± 8	137 ± 8	17 ± 14	148 ± 5	131 ± 8	17 ± 5
1650	163 ± 1	138 ± 6	25 ± 6	155 ± 4	127 ± 4	29 ± 7
1840	155 ± 7	138 ± 6	17 ± 9	153 ± 2	129 ± 7	24 ± 7
2160	157 ± 9	137 ± 6	20 ± 7	154 ± 7	129 ± 7	25 ± 11

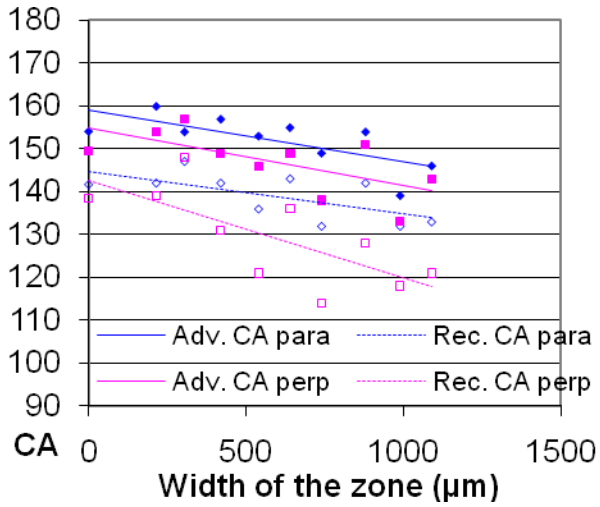

Figure 16. Advancing and receding contact angles for micropillar/nanobump-structured polypropylene surfaces with a middle zone with only nanostructure, mould temperature 50 °C. "Para" and "Perp" refer to contact angles measured parallel and perpendicular to microstructure zones.

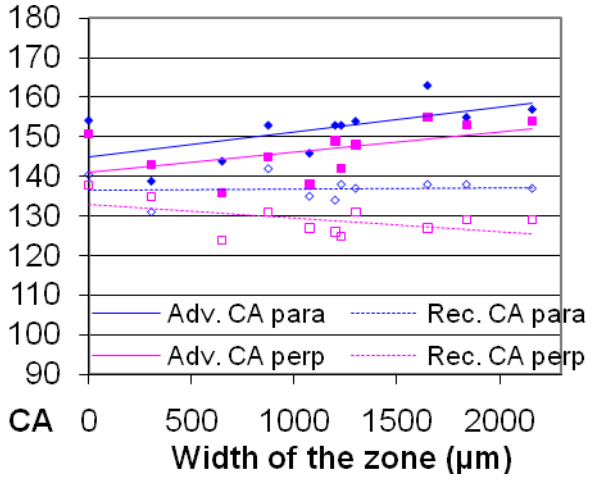

Figure 17. Advancing and receding contact angles for micropillar/nanobump-structured polypropylene surfaces with a middle zone with only nanostructure, mould temperature 70 °C. "Para" and "Perp" refer to contact angles measured parallel and perpendicular to microstructure zones.

When an anisotropic surface was achieved by creating a middle zone with hierarchical structure but where the micropillars were lower or higher than those on the edge zones (Publication IV), there still was no notable anisotropy of contact angles. Supported by both the micro- and nanostructures, the droplets maintain their symmetrical shape.

When the middle zone was lower than the edges, the nanostructure covered the micropillars more completely, and broadening of the zone led to slightly increased contact angles and decreased sliding angles in both viewing directions. The middle zone was not low enough to hinder the sliding in perpendicular direction, but the perpendicular sliding angle did not decrease as clearly as the parallel sliding angle. The nanostructure on the middle zone micropillars supported the droplets more as the zone broadened and facilitated their sliding in both directions.

When micropillars in the middle zone were higher than those in the edge zones, contact angles remained constant and sliding angles increased as the zone broadened. Since there was no nanostructure on tops of high micropillars, the droplets adhered to the pillars, and sliding was restrained.

4.4 POLYPROPYLENE SURFACES STRUCTURED WITH MICROPITS AND MICROPITS/NANODEPRESSIONS

It was expected that on pit-structured surfaces (Publication IV) water droplets would sink into the pits and contact angles would be lower. The actual effect was the reverse: the contact angles increased. With micropit–structures the dynamic contact angles were increased by 20°–30° from the values of smooth polypropylene (static CA 105°, advancing CA 107° and receding CA 91°). When the micropits were covered with nanodepressions, another 20°–30° increase was achieved. On the most hydrophobic surface the average values were static CA 149°, advancing CA 152° and receding CA 140°.

Evidently the diameters of the micropits were sufficiently small that the droplets could not sink into them but adopted the Cassie-Baxter state, resting on composite surfaces formed by the air in the pits and the polymer between the pits. On hierarchically structured surfaces, the nanodepressions between the pits and also on the pit walls further increased the proportion of air under the droplets, increasing the hydrophobicity. Theoretical contact angles were not calculated.

The dimensions of the micropits did not seem to affect the values: surfaces with very different micropit diameters and spacings had closely similar contact angles. It seemed that, rather than actual structural dimensions, it was the area fraction of the pits that correlated with the measured contact angles. With increasing area fraction of the pits, there was an increasing trend in the contact angles. Because of surface defects and variable micropit dimensions, the real area fractions of the pits that the droplets experience might differ from the estimated values and affect the contact angles. Clearly, however, the increased values stem from the created structures, not from the occasional protrusive defects.

5 CONCLUSIONS

A variety of structures on polypropylene were fabricated, in search for new methods to structure polymer surfaces and control the behaviour of water droplets on them. The effects of these structures on water were investigated with contact and sliding angle measurements.

The structuring of aluminium foils with a micro-working robot offers a quick and reliable way to fabricate mould inserts for micropillar surfaces. Both isotropic and anisotropic patterns can be created. For hierarchical structures, microstructured aluminium foils can be anodized, and with these inserts, micropillars covered with nanobumps are moulded. With proper fabrication parameters, it is also possible to create partial hierarchy where some parts of surfaces have hierarchical and other parts single-scaled structures. Pit-like structures, both on microscale and on micro/nanoscale, can be created with the help of the micro-working robot and cold mounting of epoxy to obtain the appropriate mould inserts.

Large contact angles can be achieved with micropillars, but superhydrophobic state requires hierarchical structures. On anisotropic surfaces, water will exhibit anisotropic behaviour, if the anisotropic structures and patterns are correctly proportioned. The anisotropic effect is more pronounced on surfaces with micropillars alone, but if superhydrophobicity is desired as well, structures need to be hierarchical. Because superhydrophobicity lessens the anisotropy, compromises may be required. Anisotropic surface patterns can be applied to directing and controlling the movement of water. Micropit structures increase the contact angles, and when nanoscale structure is added, superhydrophobicity is approached. A novel approach to the fabrication of hydrophobic surfaces is thereby achieved.

Artificial hierarchical pillar-like isotropic and anisotropic structures allow mimicking of the properties of the plant world. Also pit-like structures, which are rare in nature, but show similar properties to pillar surfaces, are achiavable. Through the further development of fabrication techniques, water-repellent surfaces will surely become an important part of our daily lives.

ACKNOWLEDGEMENTS

This work was carried out during the years 2006-2010 at the Department of Chemistry, University of Joensuu/University of Eastern Finland, within the Inorganic Materials Chemistry Graduate Program (EMTKO). Financial support from the Finnish Funding Agency for Technology and Innovation (TEKES) and the European Union/European Regional Development Fund is gratefully acknowledged. The work was part of the Biomimetic Nanocoatings and Nanocomposites (BNN) project. Hexion Specialty Chemicals Inc. granted me their annual chemistry student award for the year 2009.

I am deeply grateful to Prof. Tapani Pakkanen and Dr. Mika Suvanto for supervising my work. Their doors have always been open for me and my questions, even not so bright ones. Dr. Kathleen Ahonen is thanked for revisiting the language of publications I-III and this dissertation, and Dr. Mary Metzler for publication IV. Hanna-Kaisa Koponen and Esa Puukilainen introduced me to the nano- and micro-worlds and shared their expertise. The whole staff of the Department of Chemistry has provided help and companionship. Particular thanks go to Inka Saarikoski and Laura Vepsäläinen for their help, insight and spirited conversations both on and off topic.

My friends outside the university have been my bridges to the macro-world, reminding me that there are other things that matter than my surfaces. The deepest gratitude is expressed to my family: to my parents-in-law Kirsti and Seppo, who welcomed me to their home and hearts, to Dad and my sister Tuija, who have encouraged and supported me and my studies since childhood, to Titta, who as part of Dad's life has brought warmth and joy also to me, and to my husband Pertti, who has always been there for me, during the worst as well as the best of days.

Mom once said to me that her girl would always survive. Well, apparently I did. I hope she would be proud of me today.

Joensuu, December 2010

Tiina Rasilainen

REFERENCES

1 Barthlott, W., Neinhuis, C. *Planta* **202** (1997) 1.

2 Guo, Z., Liu, W., *Plant Sci.* **172** (2007) 1103.

3 Sun, T., Feng, L., Gao, X., Jiang, L. *Acc. Chem. Res.* **38** (2005) 644.

4 Feng, L., Li, S., Li, Y., Li, H., Zhang, L., Zhai, J., Song, Y., Liu, B., Jiang, L., Zhu, D. *Adv. Mater.* **14** (2002) 1857.

5 Zheng, Y., Gao, X., Jiang, L., *Soft Matter* **3** (2007) 178.

6 Gao, X., Jiang, L., *Nature* **432** (2004) 36.

7 Parker, A. R., Lawrence, C. R., *Nature* **414** (2001) 33.

8 Li, X.-M., Reinhoudt, D., Crego-Calama, M., *Chem. Soc. Rev.* **36** (2007) 1350.

9 Ma, M., Hill, R. M., *Curr. Opin. Colloid Interface Sci.* **11** (2006) 193.

10 Roach, P., Shirtcliffe, N. J., Newton, M. I., *Soft Matter* **4** (2008) 224.

11 Zhang, X., Shi, F., Niu, J., Jiang, Y., Wang, Z., *J. Mater. Chem.* **18** (2008) 621.

12 Feng, L., Zhang, Y., Xi, J., Zhu, Y., Wang, N., Xia, F., Jiang, L., *Langmuir* **24** (2008) 4114.

13 Lee, S.-M., Kwon, T.-H., *J. Micromech. Microeng.* **17** (2007) 687.

14 Lee, S.-M., Lee, H.-S., Kim, D.-S., Kwon, T.-H., *Surf. Coat. Technol.* **201** (2006) 553.

15 Sun, M., Luo, C., Xu, L., Ji, H., Ouyang, Q., Yu, D., Chen, Y., *Langmuir* **21** (2005) 8978.

16 Chen, W., Fadeev, A. Y., Hsieh, M. C., Öner, D., Youngblood, J., McCarthy, T. J. *Langmuir* **15** (1999) 3395.

17 He, B., Patankar, N. A., Lee, J. *Langmuir* **19** (2003) 4999.

18 Isenberg, B. C., Tsuda, Y., Williams, C., Shimizu, T., Yamato, M., Okano, T., Wong, J. Y. *Biomaterials* **29** (2008) 2565.

19 Jung, Y. C., Bhushan, B. *Nanotechnol.* **17** (2006) 4970.

20 Cortese, B., D'Amone, S., Manca, M., Viola, I., Cingolani, R., Gigli, G. *Langmuir* **24** (2006) 2712.

21 Puukilainen, E., Koponen, H.-K., Xiao, Z., Suvanto, S.; Pakkanen, T. A., *Colloids Surf., A* **287** (2006) 175.

22 Koponen, H.-K., Saarikoski, I., Korhonen, T., Pääkkö, M., Kuisma, R., Pakkanen, T. T., Suvanto, M., Pakkanen, T. A., *Appl. Surf. Sci.* **253** (2007) 5208.

23 Feng, L., Li, S., Li, H., Zhai, J., Song, Y., Jiang, L., Zhu, D. *Angew. Chem. Int. Ed.* **41** (2002) 1222.

24 Feng, L., Song, Y., Zhai, J., Liu, B., Xu, J., Jiang, L., Zhu, D. *Angew. Chem. Int. Ed.* **42** (2003) 800.

25 Guo, C., Feng, L., Zhai, J., Wang, G., Song, Y., Jiang, L., Zhu, D. *Chem Phys Chem* **5** (2004) 750.

26 Tuteja, A., Choi, W., Ma, M., Mabry, J. M., Mazzella, S. M., Rutledge, G. C., McKinley, G. H., Cohen, R. E. *Science* **318** (2007) 1618.

27 Disch, A., Mick, J., Bläsi, B., Müller, C. *Microsyst Technol* **13** (2007) 483.

28 Han, W., Wu, D., Ming, W., Niemantsverdriet H. (J. W.), Thüne, P. C., *Langmuir* **22** (2006) 7959.

29 Jiang, L., Zhao, Y., Zhai, J. *Angew. Chem. Int. Ed.* **43** (2004) 4338.

30 Tormen, M., Romanato, F., Altissimo, M., Businaro, L., Candeloro, P., Di Fabrizio, E. M., *J. Vac. Sci. Technol. B* **22** (2004) 766.

31 Vogelaar, L., Lammertink, R. G. H., Wessling, M. *Langmuir* **22** (2006) 3125.

32 Kim, D., Kim, J., Park, H. C., Lee, K.-H., Hwang, W. *J. Micromech. Microeng.* **18** (2008) 1.

33 Lee, Y., Park, S.-H., Kim, K.-B., Lee, J.-K. *Adv. Mater.* **19** (2007) 2330.

34 Miwa, M., Nakajima, A., Fujishima, A., Hashimoto, K., Watanabe, T., *Langmuir* **16** (2000) 5754.

35 Blossey, R., *Nat. Mater.* **2** (2003) 301.

36 Nakajima, A., Fujishima, A., Hashimoto, K., Watanabe, T., *Adv. Mater.* **11** (1999) 1365.

37 Vogler, E.A., *Adv. Colloid Interface Sci.* **74** (1998) 69.

38 Jiang, L., Feng, L. *Bioinspired Intelligent Nanostructured Interfacial Materials*, World Scientific Publishing Co. Pte. Ltd. and Chemical Industry Press, 2010, p. 122.

39 Nishino, T., Meguro, M., Nakamae, K., Matsushita, M., Ueda, Y., *Langmuir* **15** (1999) 4321.

40 Wenzel, R. N. *Ind. Eng. Chem.* **28** (1936) 988.

41 Callies, M., Quéré, D., *Soft Matter* **1** (2005) 55.

42 Cassie, A. B. D., Baxter, S., *Trans. Faraday Soc.* **40** (1944) 546.

43 Extrand, C. W. *Langmuir* **20** (2004) 5013.

44 Extrand, C. W. *Langmuir* **22** (2006) 1711.

45 Nosonovsky, N., Bhushan, B., *Ultramicroscopy* **107** (2007) 969.

46 Bhushan, B., Jung, Y. C. *Ultramicroscopy* **107** (2007) 1033.

47 Dorrer, C., Rühe, J., *Langmuir* **22** (2006) 7652.

48 Li, W., Amirfazli, A., *Adv. Colloid Interf.* **132** (2007) 51.

49 Bok, H.-M., Shin, T.-Y., Park, S. *Chem. Mater.* **20** (2008) 2247.

50 Extrand, C. W., *Langmuir* **18** (2002) 7991.

51 Li, W., Amirfazli, A. *Soft Matter* **4** (2008) 462.

52 Marmur, A., *Langmuir* **19** (2003) 8343.

53 Marmur, A., *Langmuir* **20** (2004) 3517.

54 Gao, L., McCarthy, T. J., *Langmuir* **22** (2006) 2966.

55 Nosonovsky, M., Bhushan, B., *Microelectronic Engineering* **84** (2007) 382.

56 Marmur, A., *Soft Matter* **2** (2006) 12.

57 Dorrer, C., Rühe, J., *Langmuir* **23** (2007) 3820.

58 Bico, J., Marzolin, C., Quéré, D. *Europhys. Lett.* **47** (1999) 220.

59 Fürstner, R., Barthlott, W., Neinhuis, C., Walzel, P., *Langmuir* **21** (2005) 956.

60 Nosonovsky, M., Bhushan, B., *Nano Lett.* **7** (2007) 2633.

61 Bormashenko, E., Bormashenko, Y., Stein, T., Whyman, G., Bormashenko, E., *J. Colloid Interface Sci.* **311** (2007) 212.

62 Patankar, N. A., *Langmuir* **19** (2003) 1249.

63 Gao, L., McCarthy, T. J., *Langmuir* **22** (2006) 5998.

64 Furmidge, C. G. L., *J. Colloid Sci.* **17** (1962) 309
.

65 Sakai, M., Song, J.-H., Yoshida, N., Suzuki, S., Kameshima, Y., Nakajima, A., *Surf. Sci.* **600** (2006) L204.

66 Chen, Y., He, B., Lee, J., Patankar, N.A. *J. Colloid Iinterface Sci.* **281** (2005) 458.

67 Xia, D., Brueck, S. R. J., *Nano Lett.* **8** (2008) 2819.

68 Zhao, Y., Lu, Q., Li, M., Li, X. *Langmuir* **23** (2007) 6212.

69 Hirvi, J. T., Pakkanen, T. A., *Langmuir* **23** (2007) 7724.

70 Hirvi, J. T., Pakkanen, T. A., *Surf. Sci.* **602** (2008) 1810.

71 Kusumaatmaja, H., Vrancken, R. J., Bastiaansen, C. W. M., Yeomans, J. M., *Langmuir* **24** (2008) 7299.

72 Xia, D., Brueck, S. R. J., *Nano Lett.* **8** (2008) 2819.

73 Yang, Y.-L., Hsu, C.-C., Chang, T.-L., Kuo, L.-S., Chen, P.-H., *Appl. Surf. Sci.* **256** (2010) 3683.

74 Wang, X., Berggren, M., Inganäs, O., *Langmuir* **24** (2008) 5942.

75 Yang, J., Rose, F. R. A. J., Gadegaard, N., Alexander, M. A., *Langmuir* **25** (2009) 2567.

76 Seemann, R., Brinkmann, M., Kramer, E. J., Lange, F. F., Lipowsky, R., *PNAS* **102** 82005) 1848.

77 Gao, X., Yao, X., Jiang, L. *Langmuir* **23** (2007) 4886.

78 Gao, L., McCarthy, T. J., *Langmuir* **22** (2006) 6234.

79 Gao, L., McCarthy, T. J., *Langmuir* **23** (2007) 3762.

80 McHale, G., *Langmuir* **23** (2007) 8200.

81 Panchangula, M. V., Vedantam, S., *Langmuir* **23** (2007) 13242.

82 Gao, L., McCarthy, T. J., *Langmuir* **23** (2007) 13243.

83 Choi, W., Tuteja, A., Mabry, J. M., Cohen, R. E., McKinley, G. H. *J. Colloid Interface Sci.* **339** (2009) 208.

84 Li, W., Fang, G., Li, Y., Qiao, G., *J. Phys. Chem. B.* **112** (2008) 7234.

85 Long, C. J., Schumacher, J. F., Brennan, A. B., *Langmuir* **25** (2009) 12982.

86 Zhang, F., Low, H. Y., *Langmuir* **23** (2007) 7793.

87 Onda, T., Shibuichi, S., Satoh, N., Tsujii, K., *Langmuir* **12** (1996) 2125.

88 Jokinen, V., Leinikka, M., Franssila, S., *Adv. Mater.* **21** (2009) 4835.

89 Xu, Q. F., Wang, J. N., Smith, I. H., Sanderson, K. D., *Appl. Phys. Lett.* **93** (2008) 233112-1.

90 Roberts, M. A., Rossier, J. S., Bercier, P., Girault, H. *Anal. Chem.* **69** (1997) 2035.

91 Ito, Y., Hasuda, H., Morimatsu, M., Takagi, N., Hirai, Y. J., *Biomater. Sci., Polym. Ed.* **16** (2005) 949.

92 Dang, F., Shihonara, S., Tabata, O., Yamaoka, Y., Kurokawa, M., Shihonara, Y., Ishikawa, M., Baba, Y., *Lab Chip* **5** (2005) 472.

93 Kameoka, J., Craighead, H. G., Zhang, H., Henion, J., *Anal. Chem.* **73** (2001) 1935.

94 Seddon, B. J., Shao, Y., Fost, J., Girault, H. H., *Electrochim. Acta* **39** (1994) 783.

95 Xu, J., Locascio, L., Gaitan, M., Lee, C. S., *Anal. Chem.* **72** (2000) 1930.

96 Chien, R.-D., *Sens. Actuators, A* **128** (2006) 238.

97 Rossier, J. S., Vollet, C., Carnal, A., Lagger, G., Gobry, V., Girault, H. H., Michel, P., Reymond, F., *Lab Chip* **2** (2002) 145.

98 Silva, F., Sousa, M. J., Pereira, C. M., *Electrochim. Acta* **42** (1997) 3095.

99 Wilke, S., Osborne, M. D., Girault, H. H. *J. Electroanal. Chem.* **436** (1997) 53.

100 Wilke, S., Zerihun, T., *Electrochim. Acta* **44** (1998) 15.

101 Wu, C.-H., Chen, W.-S., *Sens. Actuators, A* **125** (2006) 367.

102 Hosaka, S., Sone, H., Takahashi, Y., Shintani, T., Kato, K., Saiki, T., *Microelectron. Eng.* **67-68** (2003) 728.

103 Hosaka, S., Koyanagi, H., Katoh, K., Isshiki, F., Suzuki, T., Miyamoto, M., Arimoto, A., Maeda, T. *Microelectron. Eng.* **57-58** (2001) 223.

104 Feng, L., Zhang, Z., Mai, Z., Ma, Y., Liu, B., Jiang, L., Zhu, D. *Angew. Chem., Int. Ed.* **43** (2004) 2012.

105 Lazare, S., Tokarev, V., *Mecanique & Industries* **7** (2006) 111.

106 Moreno, P., Méndez, C., García, A., Arias, I., Roso, L. *Appl. Surf. Sci.* **252** (2006) 4110.

107 Pan, C.-T., Yang, H., Wei, M.-K., Chang, F.-Y., *Mater. Sci. Technol.* **23** (2007) 980.

108 Tokarev, V. N., Lopez, J., Lazare, S., Weisbuch, S. *Appl. Phys. A: Mater. Sci. Process.* **76** (2003) 385.

109 McHale, G., Shirtcliffe, N. J., Newton, M. I., *Analyst* **129** (2004) 284.

110 Nakajima, A., Hashimoto, K., Watanabe, T., *Monatshefte für Chemie* **132** (2001) 31.

77/2006 VENTOLA Elina: Host-guest chemistry of resorcarene derivatives studied by ESI-FTICR mass spectrometry

78/2006 HAKANPÄÄ Johanna: Structural studies of *Trichoderma reesei* hydrophobins HFBI and HFBII – the molecular basis for function of fungal amphiphiles

79/2006 ORESMAA Larisa: Synthesis, characterization and nitric oxide donation of imidazole nitrolic acids and amidoximes and their esters

80/2006 KOPONEN Markus: Noble metal promoted perovskites: reactivity and catalytic activity

81/2006 NEITOLA Raisa: *Ab initio* studies on the atomic-scale origin of friction between interacting surfaces: diamond, fluorinated diamond, graphite, and hydrocarbons

82/2006 HILTUNEN Eveliina: Phenolic extractives and discolouration of dried silver and white birch (*Betula pendula* and *Betula pubescens*) wood

83/2006 HOLOPAINEN Timo: Studies on phenol-formaldehyde resol resins for adhesives and overlays

84/2006 TURUNEN Jani: The role of mesoporous silica and alumina as metallocene catalyst supports in the formation of polyethylene nanofibers

85/2007 PUUKILAINEN Esa: Chemically modified and surface structured hydrophobic polyolefins

86/2007 KARTTUNEN Antti: Structural principles of group 14 icosahedral hydrides and elemental nanostructures of phosphorus and arsenic

87/2007 KOPONEN Hanna-Kaisa: Soiling and wetting of polymers: smooth and structured poly(vinyl chloride) and cycloolefin copolymer surfaces

88/2007 PAUNIKALLIO Teemu: Tailoring the adhesion in viscose fiber reinforced polypropylene and polyamide composites

89/2007 JAKONEN Minna: Surface-assisted synthesis of ruthenium, rhodium, and osmium carbonyl complexes, and effect of ligands on their behavior

90/2007 KOSKILINNA Jussi: Quantum chemical studies on atomic-scale tribology of diamond and boron nitride

91/2007 MARJASVAARA Asse: Mass spectrometric characterization of laccases: their catalyzing properties and molecular structure

92/2008 HIRVI Janne: Wetting of smooth and nanostructured polyethylene and polyvinylchloride surfaces studied by molecular dynamics simulations

93/2008 MIIKKULAINEN Ville: Molybdenum nitride thin films on micro- and nanopatterned substrates: atomic layer deposition and applications

94/2008 MONNI Janne: Controlled synthesis, curing, and modification of phenol-formaldehyde resol resins

95/2008 PARKKINEN Tarja: Structural studies on proteins with industrial potential: ENA11His Fab fragment, *Streptomyces rubiginosus* xylose isomerase, *Trichoderma reesei* xylanase IV and *Melanocarpus albomyces* cellobiohydrolase

96/2008 KARTTUNEN Virve: The influence of ligand structure of hafnocene catalysts on ethene polymerization studied by quantum chemical methods

97/2008 TANSKANEN Jukka: One- and two-dimensional nanostructures of group 14 elemental hydrides and group 13-15 binary hydrides

98/2009 JOKINIEMI Jonna: Structural studies on metal complexes of mixed amide esters and phenyl and monoalkyl ester derivatives of dichloromethylene biphosphonic acid

99/2009 KALIMA Valtteri: Controlled replication of patterned polymer and nanocomposite surfaces for micro-optical applications

100/2009 HYYRYLÄINEN Anna: Differentiation of diastereomeric and enantiomeric β-amino acids by mass spectrometry

101/2010 KUNNAS-HILTUNEN Susan: Synthesis, X-ray diffraction study and characterisations of metal complexes of clodronic acid and its symmetrical dianhydride derivatives

102/2010 NIEMI Merja: A molecular basis for antibody specificity – crystal structures of IgE-allergen and IgG-hapten complexes